



HAL
open science

First fossil evidence of pediculochelid mites: two new species from Middle Cretaceous and Late Eocene amber revealing morphological stasis over at least 99 million years

Vasily B Kolesniko, Dmitry D Vorontso, Roy A Norto, Pavel B Klimo

► To cite this version:

Vasily B Kolesniko, Dmitry D Vorontso, Roy A Norto, Pavel B Klimo. First fossil evidence of pediculochelid mites: two new species from Middle Cretaceous and Late Eocene amber revealing morphological stasis over at least 99 million years. *Acarologia*, 2025, *Acarologia*, 65 (1), pp.67-90. 10.24349/uxz4-s4sq . hal-04914076

HAL Id: hal-04914076

<https://hal.science/hal-04914076v1>

Submitted on 27 Jan 2025

HAL is a multi-disciplinary open access archive for the deposit and dissemination of scientific research documents, whether they are published or not. The documents may come from teaching and research institutions in France or abroad, or from public or private research centers.

L'archive ouverte pluridisciplinaire **HAL**, est destinée au dépôt et à la diffusion de documents scientifiques de niveau recherche, publiés ou non, émanant des établissements d'enseignement et de recherche français ou étrangers, des laboratoires publics ou privés.



Distributed under a Creative Commons Attribution 4.0 International License

First fossil evidence of pediculochelid mites: two new species from Middle Cretaceous and Late Eocene amber revealing morphological stasis over at least 99 million years

Vasily B. Kolesnikov ^{a,b}, Dmitry D. Vorontsov ^c, Roy A. Norton ^d, Pavel B. Klimov ^e

^a Papanin Institute for Biology of Inland Waters, Russian Academy of Sciences, 152742 Borok, Yaroslavl Province, Russia.

^b Institute of Environmental and Agricultural Biology (X-BIO), Tyumen State University, 625003 Tyumen, Russia.

^c Koltzov Institute of Developmental Biology, Russian Academy of Sciences, 119334 Moscow, Russia.

^d State University of New York, College of Environmental Science and Forestry, Syracuse, New York, USA.

^e Department of Biological Sciences, Purdue University, Lilly Hall of Life Sciences, West Lafayette, IN 47907, USA.

Original research


ABSTRACT

We present the first fossil evidence of pediculochelid mites, describing two new species: *Paralycus ekaterinae* **sp. nov.** (Eocene amber) and *P. primus* **sp. nov.** (Cretaceous amber). The exceptional preservation of the fossils, coupled with our newly developed methodological approach for examining minute arthropods in amber, has facilitated a detailed comparative morphological assessment at a resolution comparable to that of contemporary species, providing significant insights into their anatomical features. The observed morphological continuity between fossil and modern pediculochelid mites indicates the evolutionary stability of this lineage spanning at least 99 million years. These findings not only advance our knowledge of the evolutionary history of Pediculochelidae but also offer a broader perspective on the persistence of morphological traits over extensive geological timescales. We also address the phenomenon of phoresy within *Paralycus* and explore its potential implications for dispersal mechanisms. Furthermore, we evaluate the relationship between the dimensions of the amber imprints and the original size of the mites, contributing to our understanding of the mechanisms of microarthropod preservation in amber.

Received 24 September 2024

Accepted 17 January 2025

Published 27 January 2025

Corresponding author
Vasily B. Kolesnikov 
Jukoman@yandex.ru

Academic editor
Pfungstl, Tobias

<https://doi.org/10.24349/uxz4-s4sq>

ISSN 0044-586X (print)

ISSN 2107-7207 (electronic)



Kolesnikov V. B. *et al.*

Licensed under
Creative Commons CC-BY 4.0



Keywords oribatid mites; systematics; taxonomy; fossil mites; phoresy; amber imprint

Zoobank <http://zoobank.org/C5F75D45-DF99-4064-8A0F-89DE900208BA>

Introduction

The close resemblance of some Eocene oribatid soil mites from Baltic amber to extant species was first observed over 90 years ago (Sellnick 1931). Since then, extensive research has revealed a diverse array of modern mite genera preserved in both Eocene and Cretaceous amber deposits (Sidorchuk 2018; Dunlop *et al.* 2019). These findings highlight the extensive evolutionary history of mites and provide a window into the past biodiversity and ecological dynamics of these ancient ecosystems. Modern studies, employing advanced high-resolution

How to cite this article Kolesnikov V. B. *et al.* (2025), First fossil evidence of pediculochelid mites: two new species from Middle Cretaceous and Late Eocene amber revealing morphological stasis over at least 99 million years. *Acarologia* 65(1): 67-90. <https://doi.org/10.24349/uxz4-s4sq>

microscopy and imaging techniques, have provided more detailed morphological assessments of fossil mites. These techniques have further confirmed that many fossil mites from these periods display remarkable morphological similarities to their extant counterparts (Klimov *et al.* 2020; Khaustov *et al.* 2021a, b, 2024; Lindquist and Vorontsov 2023; Kolesnikov *et al.* 2023b, 2024). This high degree of morphological conservatism suggests that, despite the extensive environmental changes that have occurred over millions of years, the basic body plans and ecological niches of many mite lineages have remained relatively unchanged.

The family Pediculochelidae Lavoipierre, 1946, currently comprises a single genus, *Paralycus* Womersley, 1944, which includes 14 extant species (Kolesnikov *et al.* 2023a; Oshima *et al.* 2024; Oshima and Shimano 2024). This genus likely has a global distribution, spanning temperate to tropical latitudes (Kolesnikov *et al.* 2023a). Pediculochelid mites inhabit a wide range of environments, usually in microhabitats with low moisture levels. They have been reported from upper and deep soil layers, under pine bark, in fungal colonies on the pages of historical books, as well as in bird and bee nests; they also occur in various stored products, including *Auricularia* fungi, dried kelp, lily fruits, garlic heads, chili, walnuts, star anise, bean sticks, and even tangerine cakes (Kolesnikov *et al.* 2023a). Although records are limited, pediculochelid mites appear to use phoresy for non-host-specific dispersal, allowing them to be transported across various environments on diverse hosts. They have been documented on bees (Lavoipierre 1946; Price 1973), a ladybird beetle (Zhang and Li 2001), a rat, and even a chicken (Baker and Wharton 1952). This suggests that these mites are capable of exploiting a wide range of potential carriers for dispersal, which may facilitate their colonization of new habitats. The apparent scarcity of pediculochelid mites in collections is likely due to their minute size and inconspicuous coloration, which makes them easy to overlook, rather than an actual rarity in nature. Their ability to occupy microhabitats that are difficult to access or survey further contributes to their under-representation in scientific records. Males have not been observed in any extant species, suggesting that these mites reproduce asexually (Norton *et al.* 1983; Kolesnikov *et al.* 2023a).

Historically, Pediculochelidae has been one of the most enigmatic mite families regarding its phylogenetic placement, having been associated with nearly all major groups within the order Acariformes. When Lavoipierre (1946) first described the family, he noted its resemblance to certain members of Tarsonemidae, a highly derived family within Prostigmata. Later, Baker *et al.* (1952) reclassified Pediculochelidae under Astigmata (Acaridae), proposing it as a primitive group potentially intermediate between Astigmata and the suborder Oribatida. Without providing further justification, but likely influenced by this hypothesis, Krantz (1970) placed pediculochelid mites in the basal acariform group Endeostigmata (Pachygnathioidea). More recently, Norton *et al.* (1983) used cladistic analysis to place Pediculochelidae within Oribatida, suggesting it as the sister group to Haplochthoniidae in the basal superfamily Protoplophoroidea (Cosmochthonioidea). This phylogenetic position has since been corroborated by molecular evidence (Pepato and Klimov 2015).

Taxonomic relationships within the monogeneric family Pediculochelidae have not been thoroughly examined, likely due to a scarcity of detailed morphological information. Descriptions of adults often lack sufficient diagnostic detail, as exemplified by the type species, *Paralycus pyrigerus* (Berlese, 1905). Ontogenetic development has been fully described for only one species, *P. daeria* Kolesnikov, OConnor, Ermilov, and Klimov, 2023, and partially for three others: *P. lavoipierrei* (Price, 1973), *P. chongqingensis* Fan, Li, and Xuan, 1996, and *P. aokii* Oshima and Shimano, 2024 (Fan *et al.* 1996; Kolesnikov *et al.* 2023; Oshima *et al.* 2024). Xu *et al.* (2020) provided a key for identifying most species of the genus, excluding the poorly known *P. pyrigerus*. Subsequently, Kolesnikov *et al.* (2023a) revised this key to include *P. pyrigerus* (after examining the type specimen) along with three newly described species. This updated key expanded the range of diagnostic traits and introduced a key to identify the ontogenetic instars of the genus. More recently, the key was further supplemented with the inclusion of three additional species from Japan (Oshima and Shimano 2024). Traditionally, diagnostic characters have been largely limited to setation patterns, such as the chaetome

of the ventral idiosoma and legs, and the length of the dorsal and epimeral setae. However, Kolesnikov *et al.* (2023a) expanded the diagnostic criteria to include the shape of the solenidia on tarsus I and tibia III, providing a more comprehensive framework for species identification within this enigmatic genus and family.

To date, no fossil record of the Pediculochelidae has been documented. Here, we report two fossil species of *Paralycus* discovered in Middle Cretaceous and Late Eocene amber. Remarkably, these species exhibit only minor morphological differences from extant counterparts. Owing to their exceptional preservation and the application of a novel methodological approach for studying minute arthropods encased in amber, these fossils provide unique insights into the morphological stasis of pediculochelids over tens of millions of years.

Our objectives are to describe and formally name these two new fossil species, which could serve as valuable calibration points for constructing a time-calibrated phylogeny of the family.

Material and methods

Preparation of amber and imaging

For microscopic observation the pieces of amber were cut and polished following protocols of Sidorchuk and Vorontsov (2018). The pieces of amber were soaked in water for at least two weeks before the final imaging was done. For the holotype of *P. ekaterinae* **sp. nov.** this procedure allowed the inclusion to fill with water, making it significantly more transparent, and provided better resolution of small characters (Vorontsov and Voronezhskaya 2022, their Fig.1). Both Cretaceous specimens were initially transparent, impregnated with fossil resin.

Imaging was done with compound microscopes using brightfield and differential interference contrast (DIC) illumination: these included a Nikon E-800 with water (60×) and oil (100×) immersion optics and a Zeiss AxioImager A2 with oil immersion optics (100×). For the paratype of *P. primus* **sp. nov.** the working distance of the 100× objective was not enough to reach the whole mite when using a glass coverslip to separate amber from oil, so instead of immersion oil we used a saturated fructose solution and removed the coverslip, as described in Khaustov *et al.* (2021). Stacks of images, comprising multiple focal planes (up to 200 in a single stack), were obtained with an Olympus OM-D E-M10-II digital camera.

To obtain better resolution of minute genital structures we used a Zeiss LSM-880 confocal laser scanning microscope (CLSM) equipped with an Airyscan detector that allows significantly increased resolution (Huff 2015). Its application to the study of amber fossils is described in detail by Vorontsov and Voronezhskaya (2022) and Vorontsov *et al.* (2023). For a scan, the amber piece was immersed in saturated fructose and gently pressed onto a coverslip, which separated it from an oil immersion objective (40× or 63×).

Images were processed with Adobe Lightroom for improvement of brightness, contrast, digital noise and sharpness, and assembled from multiple focal planes using Helicon Focus 7.5. To reconstruct the outer surfaces of the inclusions, it was necessary to manually enhance the automatic focus stacking by adding significant details from individual focal planes, all performed within the same software. To manipulate the confocal image stacks the FIJI software package (Schindelin *et al.* 2012) was used. Drawings were prepared using Adobe Photoshop, with image stacks serving as a background, as described by Coleman (2006). The original image stacks are available through Figshare (<https://doi.org/10.6084/m9.figshare.27086758>).

Terminology and measurements

Measurements are given in micrometers (µm) and were taken from edge to edge of a structure in its widest part. Where possible, setae were measured when oriented perpendicularly to the optical axis of the microscope. Since in most cases the orientation of structures was sub-optimal, all measurements are to be treated as minimal estimates and are rounded to the closest 5 if over 50. Leg setation formulas (including famulus) are provided in brackets, following the

sequence: trochanter-femur-genu-tibia-tarsus. Leg solenidia formulas are presented in square brackets, following the sequence: genu-tibia-tarsus. Morphological terminology used in this paper follows that of F. Grandjean (see Norton *et al.* 1983 for review and application).

The following abbreviations are used. *Prodorsum*: *ro*, *le*, *in*, *exa*, *exp*, *bs* = rostral, lamellar, interlamellar, anterior exobothridial, posterior exobothridial and bothridial seta, respectively. *Notogaster*: *C*, *DE*, *F*, *H*, *PS* – notogastral segments; *c*, *d*, *e*, *f*, *h*, *p* = notogastral setae; *tf* = transverse furrows; *ia*, *im*, *ip*, *ih*, *ips* = notogastral cupules. *Gnathosoma*: *a*, *m*, *h* = subcapitular setae; *or* = adoral seta; *sup*, *inf*, *d*, *acm*, *ul*, *sul*, *vt*, *lt* = palp setae; ω = palp solenidion; *e* = supracoxal setae; *cha*, *chb* = cheliceral setae. *Epimeral and lateral podosomal regions*: *1a*, *1b*, *1c*, *2a*, *2b*, *3a*, *3b*, *3c*, *4a*, *4b*, *4c* = epimeral setae. *Anogenital region*: *g*, *eg*, *an*, *ad* = genital, eugenital anal and adanal setae, respectively. *Legs*: *Tr*, *Fe*, *Ge*, *Ti*, *Ta* = leg trochanter, femur, genu, tibia, and tarsus, respectively; ω , ϕ , σ = leg solenidia; ε = leg famulus; *d*, *l*, *v*, *bv*, *ev*, *ft*, *p*, *u*, *a*, *s*, *m*, *it*, *tc*, *pv* = leg setae.

Systematic paleontology

Class Arachnida Cuvier, 1812

Order Sarcoptiformes Reuter, 1909

Suborder Oribatida Dugès, 1834

Family Pediculochelidae Lavoipierre, 1946

Genus *Paralycus* Womersley, 1944

Type species — *Alycus pyrigerus* Berlese, 1905, by original designation.

Paralycus ekaterinae sp. nov.

Zoobank: [1EB90655-45C2-4EC7-9908-7E1604BAF111](https://zoobank.org/1EB90655-45C2-4EC7-9908-7E1604BAF111)

(Figs. 1–6)

Material and type repository

The piece of Eocene amber (original weight 1.92 g) containing the holotype of *Paralycus ekaterinae* sp. nov. was mined in the Pugach quarry (Klesov, Ukraine) and obtained from the “Ukramber» factory. The amber is dated to the Priabonian Age (33.9–37.8 Mya) of the Late Eocene (Perkovsky *et al.* 2010; Sokoloff *et al.* 2018, Radchenko *et al.* 2021).

Holotype: A piece of amber, approximately parallelepiped in shape, measuring $2.4 \times 0.5 \times 0.2$ mm. It is housed in the amber collection of the Schmalhausen Institute of Zoology, NAS of Ukraine, in Kiev, with the collection number SIZK K-7664-II. Embedded in epoxy resin between two round glass coverslips. Syninclusions: K-7663 Carabidae; K-7663a legs of Nematocera; K-7663b spider silk; K-7664 Chironomidae, Orthoclaadiinae female.

Diagnosis

Body size: 166×61 . Rostral setae short, shorter than half length of chelicera. Notogastral setae short, d_2 , e_1 , f_1 not reaching base of next setal row; h_1 reaching base of p_1 . Seta p_2 longer than other notogastral setae. Setal formula of epimeres: 3–2–3–2 (*4a* absent). Seta *2a* not reaching base of *1a*. Five pairs of genital setae. Genua with 4–2–0–0 setae, trochanters with 0–0–1–0 setae. Cheliceral setae *cha* and *chb* short.

Description

Presumably adult female. Minute, elongate, weakly sclerotized. Length of idiosoma 142, width 61, body length including gnathosoma 166, prodorsum length 24, prodorsum width 40. Prodorsal shield and legs smooth. Notogaster and ventral side of body striated.

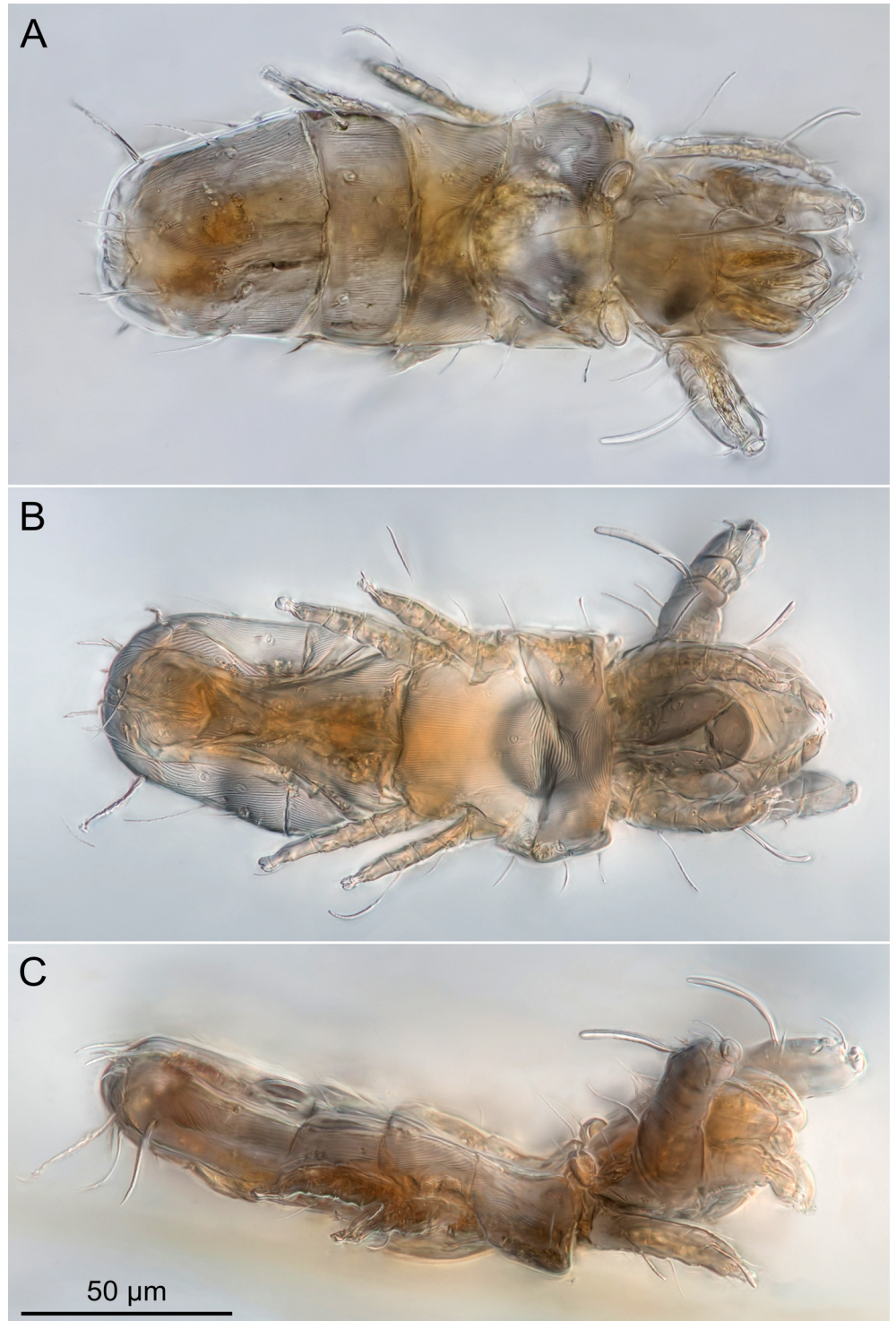


Figure 1 . *Paralycus ekaterinae* sp. nov., SIZK K-7664-II, holotype, focus-stacked DIC micrographs, total view. A – dorsal aspect; B – ventral aspect; C – lateral aspect. The specimen was imaged after soaking the polished piece of amber in water for several days. However, in the ventral aspect, an air bubble is still visible inside the inclusion as a darker shadow.

Gnathosoma (Figures 1, 2A, 3, 4) — Subcapitulum 19×29 , length underestimated. Structures of subcapitulum and rutellum poorly visible, following setae observed: *a* (4), *h* (5) and left *m* (5), *or*₂ (4) and right *or*₁ (3) (contralateral *or*₁ probably hidden below *or*₂). Palp (29)

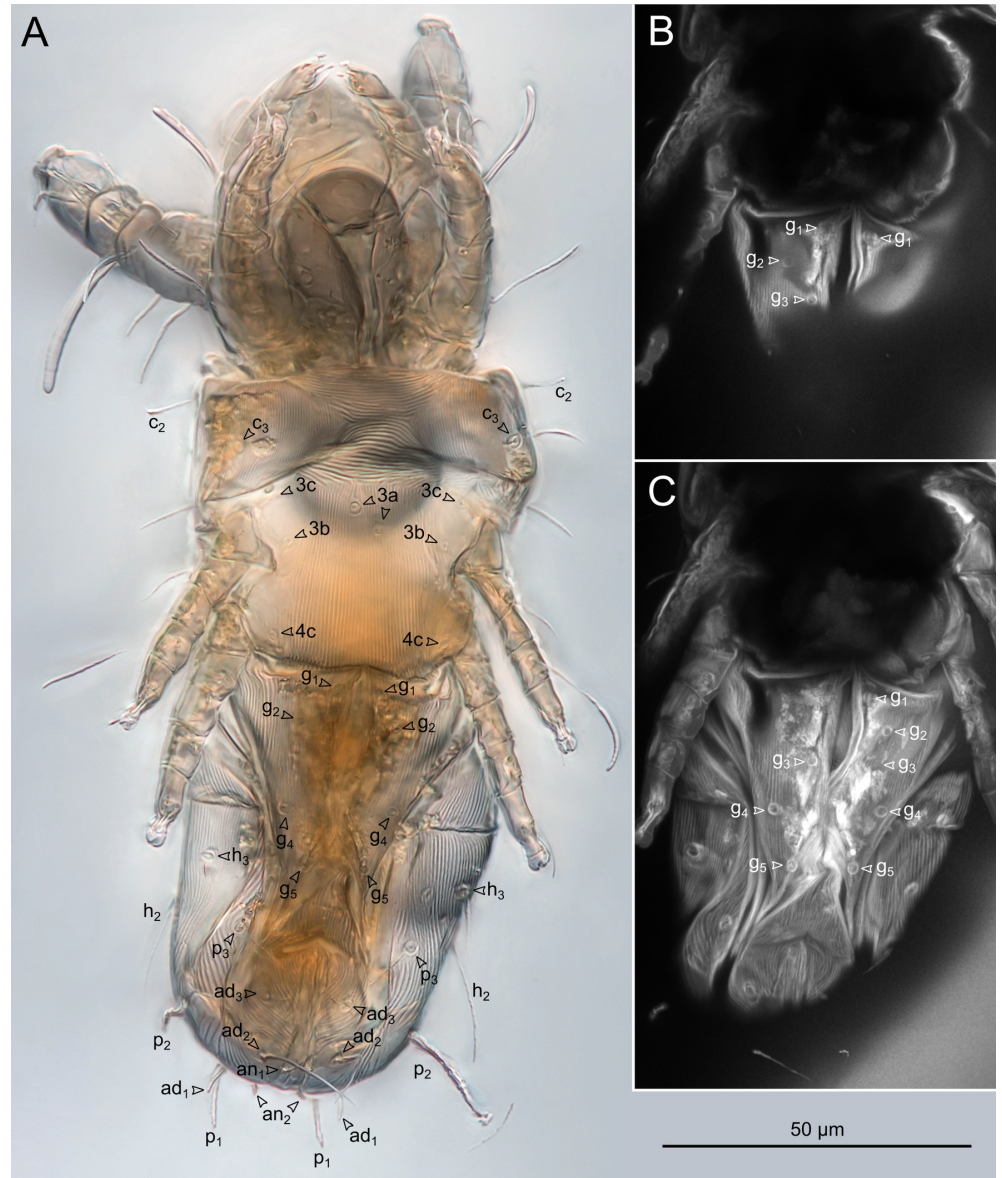


Figure 2 . *Paralycus ekaterinae* sp. nov., SIZK K-7664-II, holotype, ventral aspect. A – manually focus-stacked DIC micrograph showing the surface of the amber imprint. The amber piece was soaked in water to enhance transparency. Despite several attempts, genital setae *g3* could not be reliably visualized; B – a single frame from the confocal image stack of the same specimen, using a 488 nm excitation laser, Airyscan mode. The alveoli of setae *g1–g3* are clearly visible; C – maximum intensity projection obtained from the same image stack, aligned with the photo on the left (A). Note that some of the alveoli visible in (B) are obscured by other cuticular remnants that exhibit brighter autofluorescence. In most cases, setae could be distinguished from other objects in the confocal stack by tracing them through multiple layers (see the source image stacks provided as a supplement to this paper).

with four free segments (femur and genu immovably fused, although partial suture delineates them); setal formula, including ω : 0–2–0–1–7. Supracoxal seta *e* above base of palp poorly visible. Chelicera large (24), with two setiform smooth setae *cha* (7) and *chb* (poorly visible). Fixed digit of chelicera with three teeth, one tooth distinctly larger than others; movable digit with three teeth of approximately equal size, deep furrow between lateral teeth present.

Prodorsum (Figures 1A, 3) — Prodorsum covered with shield-shaped plate in mid-dorsal region, bearing two pairs of setae, *ro* (7) and *le* (14). With two other pairs of setae—*exa*

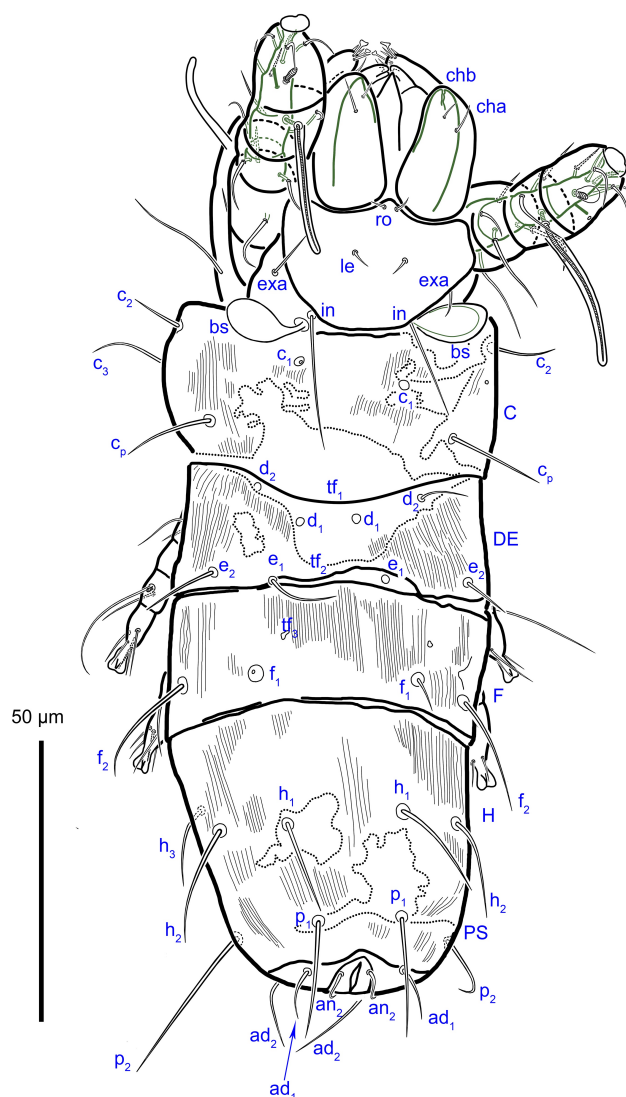


Figure 3 . *Paralycus ekaterinae* sp. nov., drawing, dorsal aspect. The green outline in the anterior part of the mite indicates the borders of cuticular structures visible within the larger amber imprint.

(13) and *in* (24)—and one pair of clavate bothridial setae (*bs*, 15 × 7) in dorsolateral area of prodorsum; *exp* not clearly visible, but probably present hidden below bothridial setae.

Gastronotum (Figures 1A, 3) — *Gastronotum* divided into four regions by three transverse furrows (*tf*₁₋₃). Segment *C* bears four pairs of setae: *c*₁ (only alveoli observed), *c*₂ (12), *c*₃ (15, left seta well visible ventrally, but only alveolus visible on right side) and *c*_p (18). Compound segment *DE* bears four pairs of setae: *d*₁ (only alveoli observed), *d*₂ (10, only alveolus visible on left side), *e*₁ (12) and *e*₂ (15). Segment *F* bears two pairs of setae: *f*₁ (18-20) and *f*₂ (21). Segments *H* and *PS* merged and bear six pairs of setae: *h*₁ (19), *h*₂ (21), *h*₃ (15, right visible only ventrally), *p*₁ (22), *p*₂ (30) and *p*₃ (10, visible only ventrally). Seta *p*₂ longer than other notogastral setae. Seta *d*₂ does not reach base of *e*, *e*₁ does not reach base of *f*₁, *f*₁ does not reach base of *h*₁, *h*₁ reaches base of *p*₁. Cuticle of segments *C*, *DE*, *F*, *H* and *PS* damaged medially.

Epimeral region (Figures 2A, 4) — Setal formula of epimeres: 3–2–3–2. Setae *1a* (4), *1b* (8), *2a* (5), *2b* (15), *3b* (6), *3c* (4) and *4c* (5) setiform, smooth. Setae *1c* and *3a* observed as

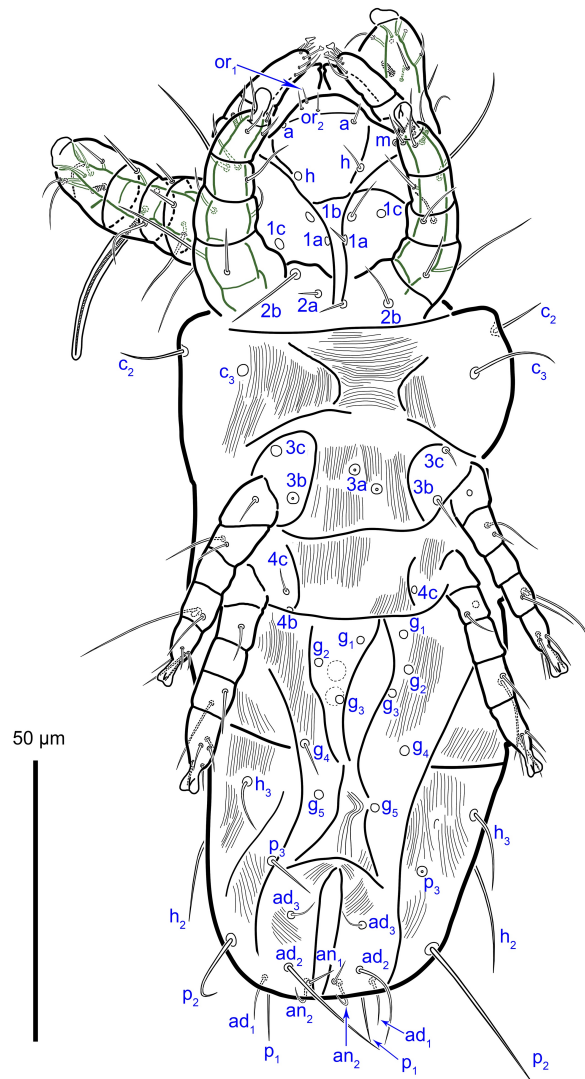


Figure 4 . *Paralycus ekaterinae* sp. nov., drawing, ventral aspect. The green outline in the anterior part of the mite highlights the cuticular structures within the larger amber imprint.

alveoli. Seta *3a* situated close to each other, seta *4a* absent.

Anogenital region (Figures 2, 4) — With five pairs of genital setae (or their alveoli); and two genital papillae clearly visible; setae *eg* poorly visible. Three pairs of adanal setae: *ad*₁ (10), *ad*₂ (23) and *ad*₃ (7); two pairs of anal setae: *an*₁ (6) and *an*₂ (9, bent ventrally).

Legs (Figures 1, 2A, 5, 6, Tables 1, 2) — Legs short. Tarsus I elongated. Amber imprints of legs I and II probably swollen during fossilization (see Discussion section). Cuticular remnants of legs observed inside the imprint. All leg segments present. Claws absent on all tarsi, each tarsus with minute empodial remnant and caruncle-like membrane. Formulas of leg setation and solenidia (homologies of setae and solenidia indicated in Table 2): I (0–2–4–2–9) [0–1–1], II (0–2–2–3–6) [0–0–1], III (1–2–0–2–5) [0–1–0], IV (0–2–0–2–5) [0–0–0]. All setae filiform, smooth. Unguinal setae *u* and proral setae *p* on tarsi I–IV simple; *p'* and *p''* poorly visible on some legs. Seta *l'* on left tibia II not observed, seta *d* on femur IV observed as alveolus. Solenidion ω on tarsi I–II short, baculiform; solenidion ϕ on tibia I elongate, attenuate; ϕ on tibia III short, expanded at end. All genua, tibia II and IV, tarsus IV lacking solenidia. Famulus

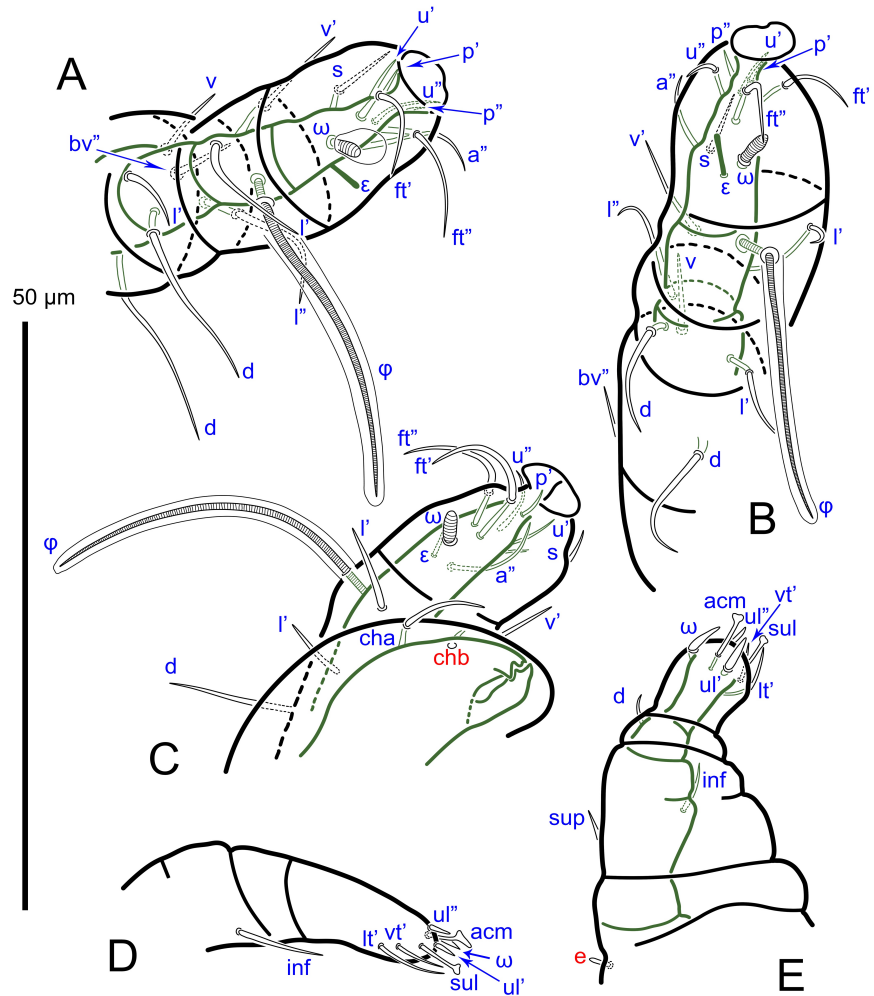


Figure 5. *Paralycus ekaterinae* sp. nov., drawings. A – right leg I, dorsal aspect; B – left leg I, dorsal aspect; C – left chelicerae and part of left leg I, paraxial view; D – part of right palp, ventral aspect; E – left palp, antiaxial view. The green outline shows the cuticular structures inside the larger amber imprint. Structures that are poorly visible in the fossil but are expected to be present are indicated in red.

ϵ baculiform, thin. Length of setae on femur I: d 17, bv'' 7. Length of setae on genu I: d 14, l' 6, v 7. Length of setae and solenidium on tibia I: l' 10, v' 10, ϕ 28. Length of setae and solenidium on tarsus I: ft' 9, ft'' 10, s 7, a'' 8, u 5, p 3, ϵ 4, ω 3. Length of setae on femur II: d 19, bv'' 8. Length of setae of genua II: l' 9, l'' 7. Length of setae on tibia II: d 20, l' 11, v' 10. Length of setae and solenidium on tarsus II: ft' 7, u 6, p 3, ω 3. Length of seta v' on trochanter III 5. Length of setae on femur III: d 12, ev' 7. Length of setae and solenidium on tibia III: d 22, v' 10, ϕ 2. Length of setae on tarsus III: ft'' 10, u 7, p 5. Length of seta ev' on femur IV 7. Length of setae on tibia IV: d 15, v' 8. Length of setae on tarsus IV: ft'' 7, u 6, p 5.

Etymology

Paralycus ekaterinae is named after the late Ekaterina Sidorchuk who pioneered the high-resolution study of fossil Acari.

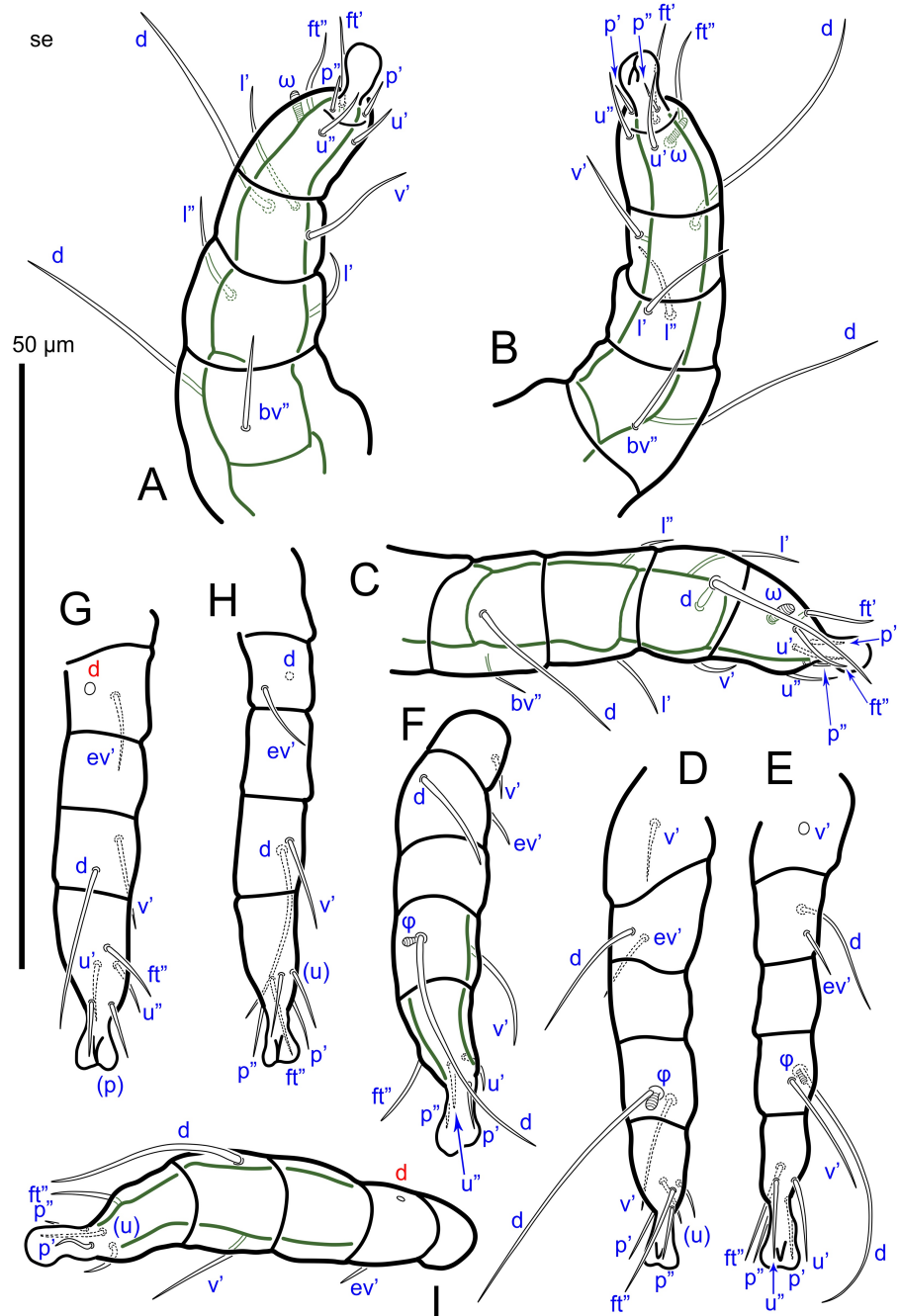


Figure 6 . *Paralycus ekaterinae* sp. nov., drawings. A – right leg II, ventral aspect; B – left leg II, ventral aspect; C – left leg II, antiaxial view; D – right leg III, dorsal aspect; E – left leg III, ventral aspect; F – left leg III, antiaxial view; G – right leg IV, dorsal aspect; H – left leg IV, ventral aspect; I – left leg IV, antiaxial view. The green outline shows the cuticular structures inside the larger amber imprint. Structures that are poorly visible in the fossil but are expected to be present are indicated in red.

Remarks

Among the known *Paralycus* species, *P. ekaterinae* sp. nov. is morphologically similar to *P. nortoni* (Xu et al. 2020) by the absence of setae *4a* between epimeral plates IV and by the presence of five pairs of genital setae. *Paralycus ekaterinae* sp. nov. differs from *P. nortoni*

Table 1 . Leg lengths of *Paralycus ekaterinae* sp. nov.

Leg	Trochanter	Femur	Genu	Tibia	Tarsus	All	Leg to body length ratio
I	6	10	6	9	15	46	≈0.28
II	5	8	6	7	12	38	≈0.22
III	9	9	6	7	8	39	≈0.23
IV	7	7	8	9	10	41	≈0.25

Note: Measurements are given in micrometers (µm) and are to be treated as minimal estimates.

Table 2 . Leg setation of *Paralycus ekaterinae* sp. nov.

Leg	Trochanter	Femur	Genu	Tibia	Tarsus
I	-	<i>bv''</i> , <i>d</i>	(<i>l</i>), <i>v</i> , <i>d</i>	<i>l'</i> , <i>v'</i> , φ	(<i>ft</i>), <i>a''</i> , <i>s</i> , (<i>u</i>), (<i>p</i>), ω, ε
II	-	<i>bv''</i> , <i>d</i>	(<i>l</i>)	<i>l'</i> , <i>v'</i> , <i>d</i>	(<i>ft</i>), (<i>u</i>), (<i>p</i>), ω
III	<i>v'</i>	<i>ev'</i> , <i>d</i>	-	<i>v'</i> , <i>d</i>	<i>ft''</i> , (<i>u</i>), (<i>p</i>)
IV	-	<i>ev'</i> , <i>d</i>	-	<i>v'</i> , <i>d</i>	<i>ft''</i> , (<i>u</i>), (<i>p</i>)

Note: Roman letters refer to normal setae, Greek letters refer to solenidia (except ε = famulus); *d*ϕ – coupled seta and solenidion. Single prime (') and double prime (") indicate setae on the anterior and posterior side of a segment, respectively. Parentheses indicate paired setae (' and ").

by the following: there are two setae *l* on genu II (two *l* and one *d* in *P. nortoni*), rostral seta *ro* is shorter than half the length of the chelicera (longer in *P. nortoni*), seta *f*₁ is not reaching the base of *h*₁ (reaching in *P. nortoni*). Seta *4a* is also absent between epimeral plates IV in *P. parvulus* (Price, 1973), but that species has three pairs of genital setae (vs. five in *P. ekaterinae* sp. nov.), while its notogastral setae and seta *ro* are distinctly longer (setae *d*₂, *e*₁, *f*₁ reach base of next setal row, *ro* reach half the length of the chelicera) than in *P. ekaterinae* sp. nov. (*d*₂, *e*₁, *f*₁ not reaching base of next setal row and *ro* not reaching half the length of the chelicera). *P. longior* Fan, Li and Xuan, 1996 also has five pairs of genital setae, but it has setae *4a*, and seta *ro* is longer than half the length of the chelicera.

Price (1973) designated two paratypes of *P. raulti* (Lavoipierre, 1946) that differed by the number of genital setae (four in specimen #1 and five in specimen #2) and by the length of setae *ro* and *cha* (longer in specimen #2). Kolesnikov *et al.* (2023a) demonstrated that specimen #1 is a separate species, and described it as *P. pricei* Kolesnikov, OConnor, Ermilov and Klimov, 2023, and specimen #2 was retained as *P. raulti*. *Paralycus ekaterinae* sp. nov. differs from *P. raulti* by the following: seta *4a* are absent (present in *P. raulti*), setae *cha* and *ro* are distinctly shorter (not reaching half the length of the chelicera) than in *P. raulti* (reach half the length of the chelicera).

***Paralycus primus* sp. nov.**

Zoobank: 913F1204-10A0-4975-96C6-9A72AAE0DC92

(Figs. 7–13)

Material and type repository

The piece of Cretaceous amber containing the holotype and single paratype of *Paralycus primus* sp. nov. was mined in the Hukawng Valley of northern Myanmar (Kachin State). The Kachin amber locality was radiometrically dated to 98.79 ± 0.62 Ma based on U–Pb zircon dating of the volcanoclastic matrix and shown to be earliest Cenomanian in age (Shi *et al.* 2012; Smith and Ross 2018; Zhang *et al.* 2018; Yu *et al.* 2019).

Holotype (piece of amber, approximate parallelepiped 2.0 × 1.7 × 0.3 mm, collection number PIN 5620-90 E) and one paratype (piece of amber of uneven shape 5.0 × 3.3 × 2.8 mm, collection number PIN 5620-90 D). Specimens are housed in the Öhm-Kühnle collection

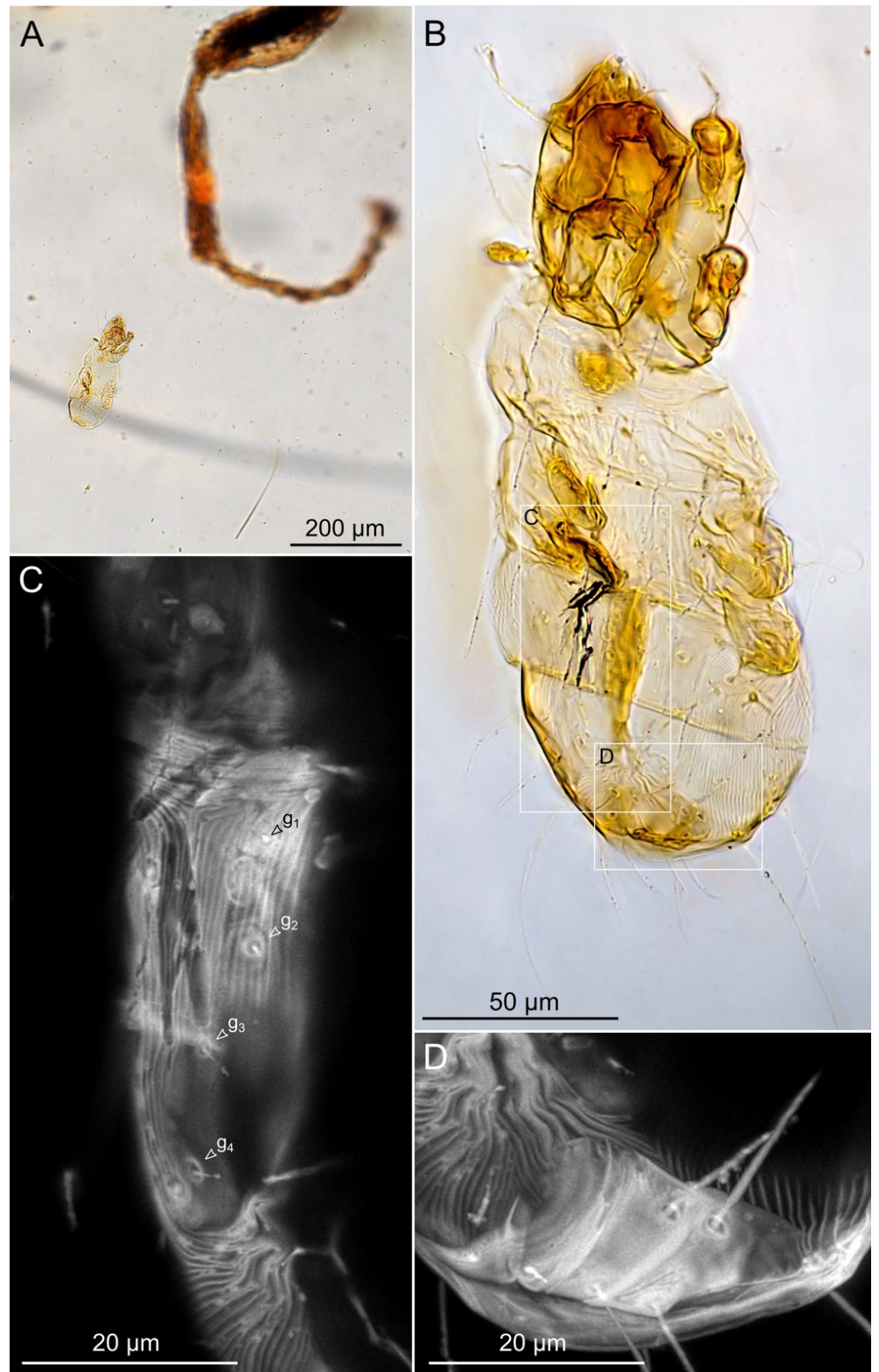


Figure 7. *Paralycus primus* sp. nov., micrographs of PIN 5620-90 D, paratype. A – the mite is situated very close to a leg of a wasp, which limited the possible observation aspects; B – ventral aspect, focus-stacked total view, DIC image; C, D – maximum intensity projections of confocal image stacks (Airyscan mode), highlighting the higher resolution of the genital and anal regions, respectively.

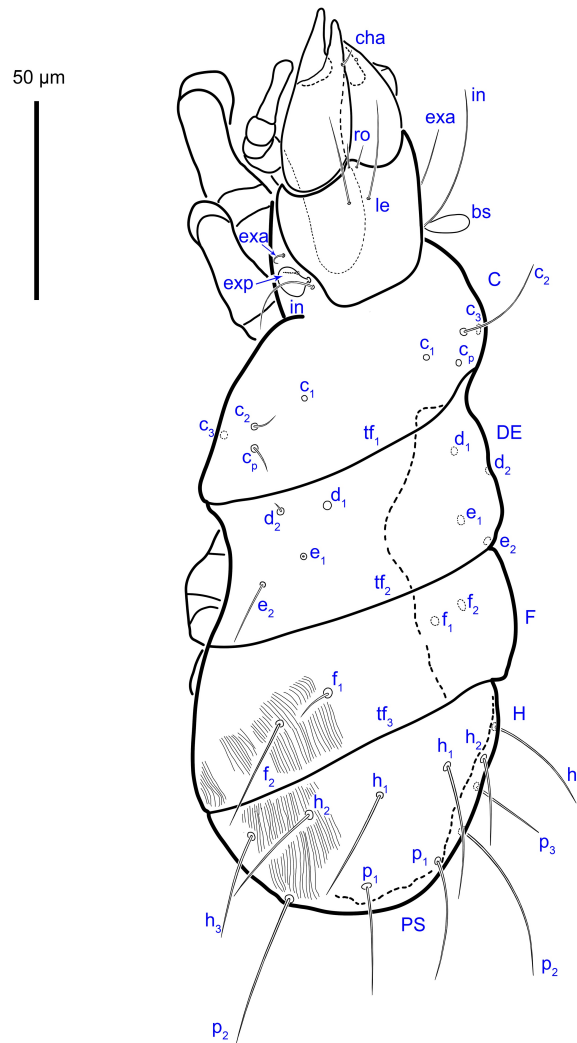


Figure 8 . *Paralycus primus* **sp. nov.**, paratype, drawing, dorsal aspect.

maintained permanently at the A.A. Borissiak Paleontological Institute, Russian Academy of Sciences, Moscow. The holotype is embedded in epoxy resin between two round glass coverslips. The paratype is not separated from the syninclusion (Chrysoidea wasp, PIN 5620-90 A) and is located approximately 150–200 µm from its foreleg (Fig.7A). The amber piece is trimmed and polished to provide access to the mite from its ventral and lateral sides.

Almost all inclusions in the piece of amber, including *Paralycus* mites, are completely impregnated with fossil resin, which is typical for Kachin amber, and there are no air-filled imprints (unlike *P. ekaterinae* **sp. nov.** and many other amber fossils).

Syninclusions: PIN 5620-90 A (Hymenoptera: Chrysoidea fam. indet. cf. *Nadezhdaabythus* Zhang *et al.* 2020), PIN 5620-90 B (Homoptera: Coccoidea male); many fragments of presumably arthropod origin.

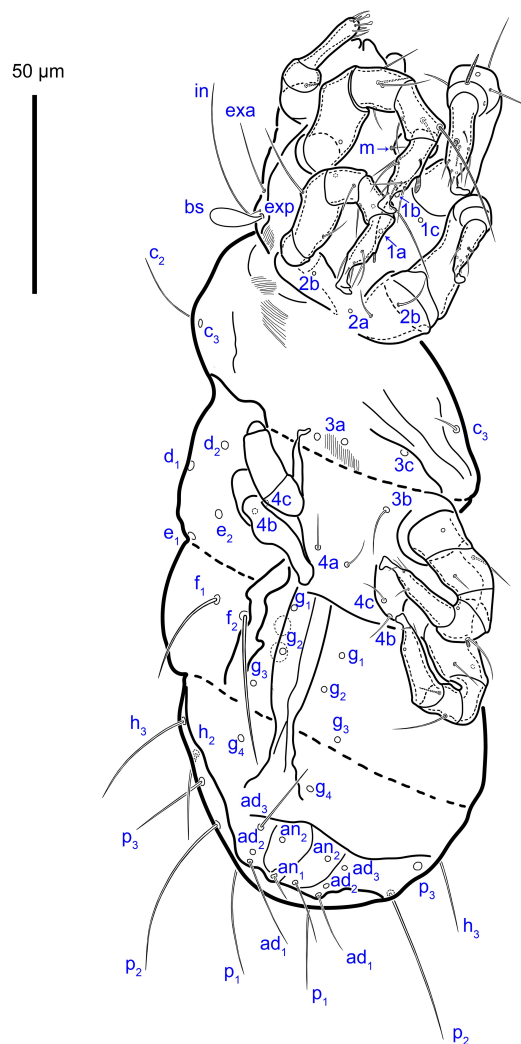


Figure 9 . *Paralycus primus* sp. nov., paratype, drawing, ventral aspect.

Diagnosis

Body 190–210 × 65–80. Rostral seta shorter than half length of chelicera. Notogastral setae long, d_1 , d_2 , e_1 , f_1 , h_1 reaching bases of respective seta in next posterior row. Seta p_2 longer than other notogastral setae. Setal formula of epimeres: 3–2–3–3 ($4a$ present); seta $2a$ not reaching $1a$. Four pairs of genital setae. Genua with 4–2–0–0 setae, trochanters with 0–0–1–0 setae. Cheliceral seta cha and chb short. One pair of subcapitular setae m .

Description

Presumably adult females. Minute, elongate, weakly sclerotized. Length of idiosoma 160–196, width 65–80, body length including gnathosoma 190–210, prodorsum length 37–38, prodorsum width 32–37. Prodorsal shield of and legs smooth. Notogaster and ventral body finely striated.

Gnathosoma (Figures 11A, 12, 13) — Subcapitulum well-visible only in holotype, base wide base (distorted), rutellum observed, setae h (9), a , m , or_1 (5) and or_2 (8) observed, m_2 absent; in paratype, only area of seta m (5) observed. Palp (33) four-segmented (femur and

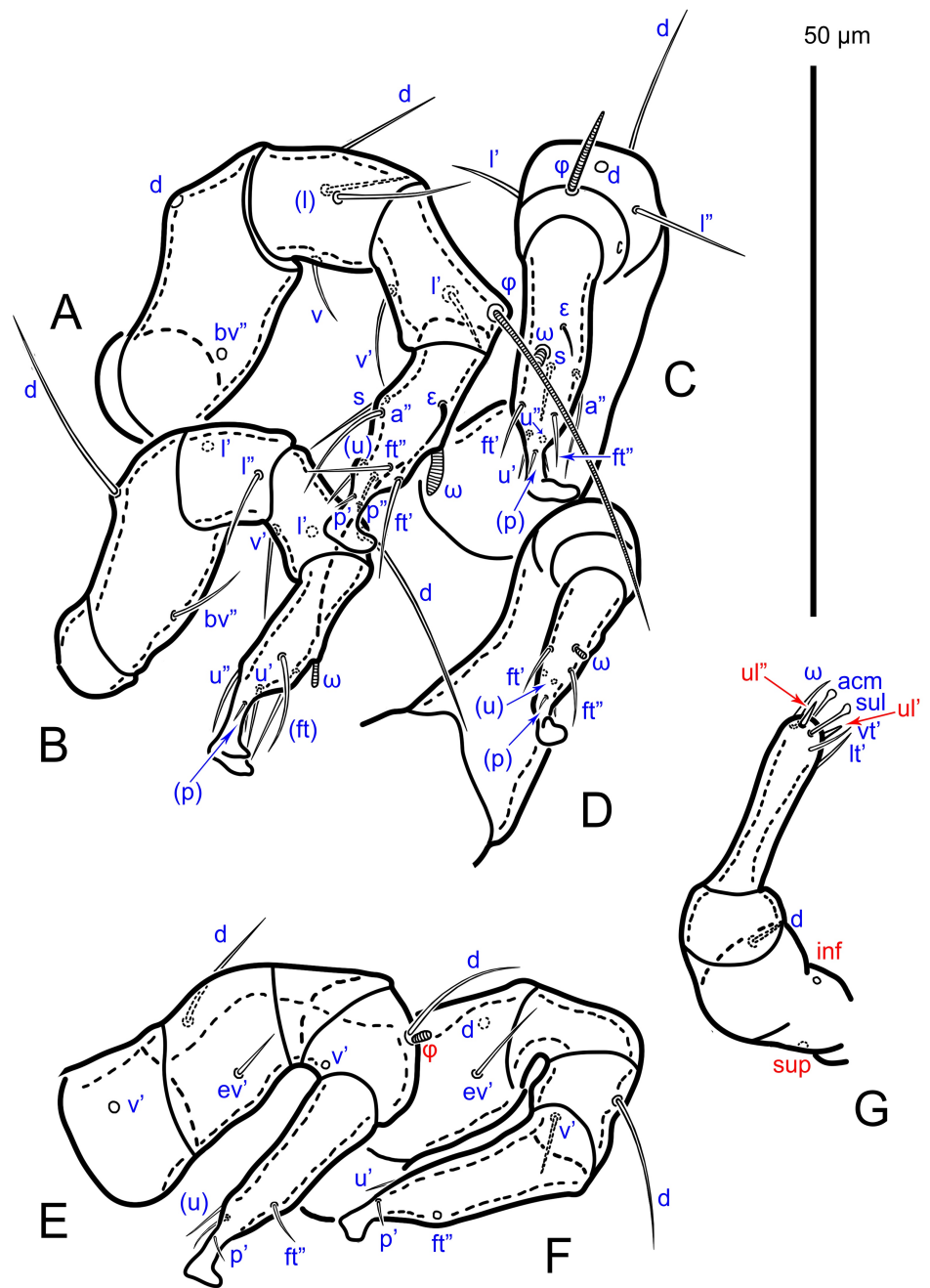


Figure 10 . *Paralycus primus* sp. nov., paratype, drawings. A – right leg I, antiaxial view; B – right leg II, antiaxial view; C – left leg, dorsoventral view; D – left leg II, dorsoventral view; E – left leg III, antiaxial view; F – left leg IV, antiaxial view; G – right palp, ventroantiaxial view. Structures that are poorly visible in the fossil but are expected to be present are indicated in red.

genus immovably fused, although partial suture delineates them); setal formula (in holotype only femoral setae visible), including ω : 0–2–0–1–7 (setae *ul* poorly visible). Chelicera large

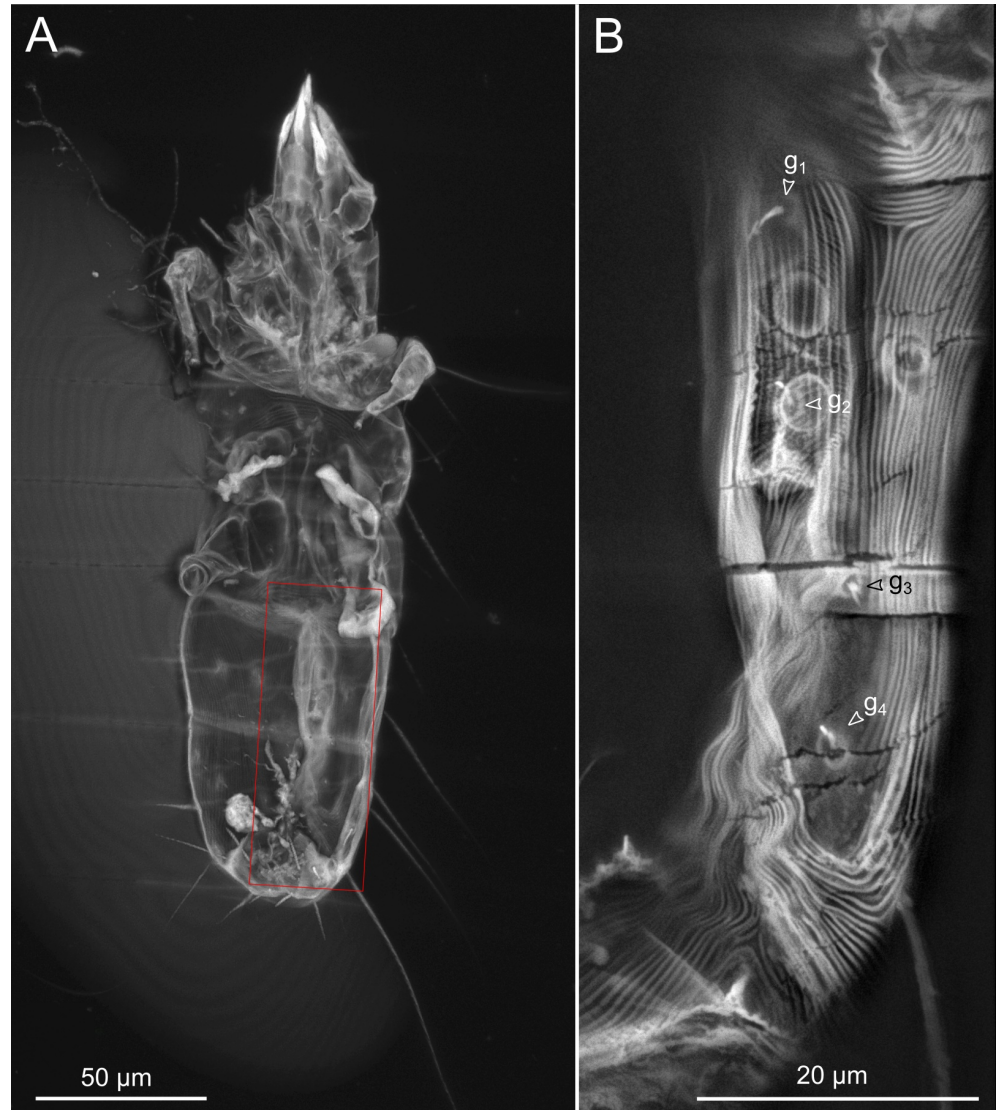


Figure 11 . *Paralycus primus* sp. nov., micrographs of PIN 5620-90 E, holotype. A – ventral aspect, maximum intensity projection of confocal image stack, 488nm excitation laser; B – genital area scanned with a higher resolution (Airyscan mode), focus-stacked confocal images.

(45–47), with two setae: *cha* (5–10) and *chb* (8, visible only unilaterally in holotype).

Prodorsum (Figures 8, 12) — Prodorsum covered with shield-shaped plate in mid-dorsal region, bearing two pairs of setae, *ro* (7) and *le* (24). With three other pairs of setae *exa* (20), *in* (40–56), *exp* (4, not visible in holotype) and one pair of clavate bothridial setae (*bs*, 15 × 8–9) in dorsolateral area of prodorsum.

Gastronotum (Figures 7B, 8, 12) — Gastronotum divided into four regions by three transverse dorsal sutures. Segment *C* bears four pairs of setae: *c*₁ (10), *c*₂ (20–25), *c*₃ (20, on ventral side) and *c*_p (36–38). Compound segment *DE* bears four pairs of setae: *d*₁ (25), *d*₂ (16), *e*₁ (33) and *e*₂ (17–29); in holotype, right setae *d*₂ and *e*₂ not observed. Segment *F* bears two pairs of setae: *f*₁ (35) and *f*₂ (30–40). Segments *H* and *PS* fused and bear six pairs of setae: *h*₁ (35–39), *h*₂ (30–40), *h*₃ (30–35), *p*₁ (31–35), *p*₂ (40–80) and *p*₃ (20–22). Seta *p*₂ slightly longer than other notogastral setae. Seta *d*₁ reaches base of *e*₁, *d*₂ reaches base of *e*₂, *e*₁ reaches base of *f*₁, *f*₁ reaches base of *h*₁, *h*₁ reaches base of *p*₁.

Epimeral region (Figures 9, 11A, 13) — Setal formula of epimeres: 3–2–3–3. Setae *Ib* (8),

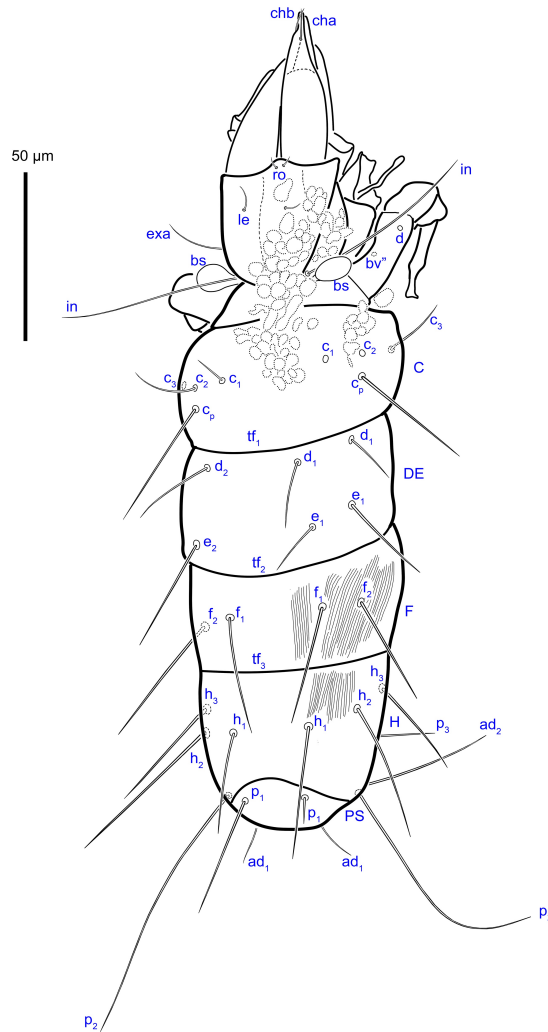


Figure 12 . *Paralycus primus* sp. nov., holotype, drawing, dorsal aspect.

2a (8), 2b (11), 3b (12) and 4a (9), 4b (7), 4c (7) filiform, smooth; other setae observed only as alveoli. Distance between setae 3a shorter than that of setae 4a.

Anogenital region (Figures 7C, D, 9, 11, 13) — Four pairs of genital setae, situated at approximately equal distances from each other. Two pairs of genital papillae visible, setae *eg* not observed. Three pairs of adanal setae: *ad*₁ (12–24), *ad*₂ (46) and *ad*₃ (14–19); two pairs of anal setae: *an*₁ (8) and *an*₂ (12–16).

Legs (Figures 10, 13, Tables 3, 4) — Holotype lacks legs I, other legs poorly visible. In paratype, right legs I–II and left legs III–IV clearly visible. Legs short, tarsus I elongated. Claws absent on all tarsi; each tarsus with minute empodial remnant and caruncle-like membrane. Formulas of leg setation and Solenidia (homologies of setae and solenidia indicated in Table 4): I (0–2–4–2–9) [0–1–1], II (0–2–2–3–6) [0–0–1], III (1–2–0–2–5) [0–1–0], IV (0–2–0–2–5) [0–0–0]. All setae filiform, smooth. Unguinal seta *u* and proral seta *p* on tarsus I–IV simple (setae *p*'' on tarsus III–IV, and *u*'' on tarsus IV not visible). Setae *d*, *bv*'' on right femur I, *l*' on right genu and tibia II, *v*' on left trochanter and tibia III, *d* on femur IV and *ft*'' on tarsus IV visible only as alveoli. Solenidion ω on tarsus I–II short, baculiform; solenidion φ on tibia I elongate, attenuate; φ on tibia III short, expanded on end. All genua, tibiae II and IV, tarsus IV without solenidia. Famulus ε baculiform, thin. Seta *d* of femur I 15. Length of setae on genu I:

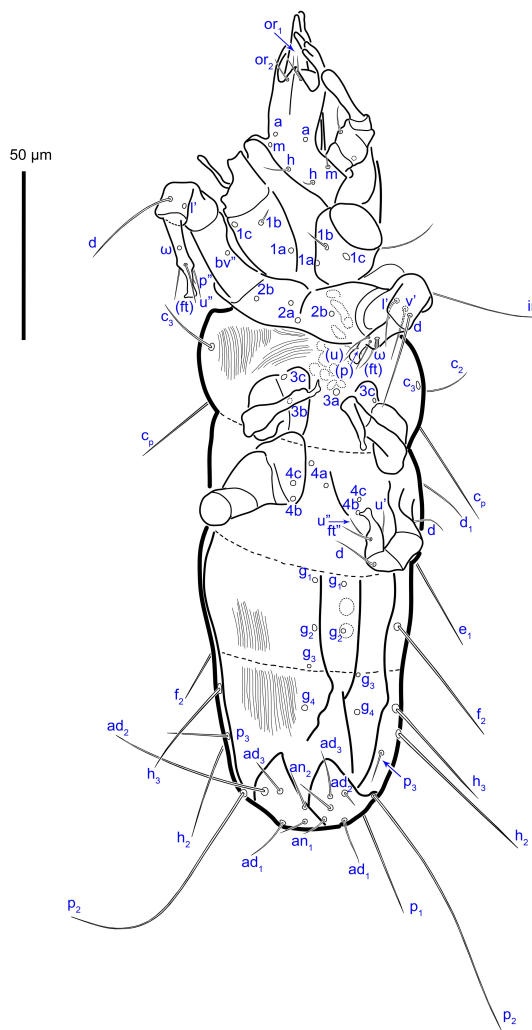


Figure 13 . *Paralycus primus* sp. nov., holotype, drawing, ventral aspect.

d 11, *l'* 8, *l''* 12, *v* 7. Length of setae and solenidion on tibia I: *l'* 7, *v'* 10, ϕ 32. Length of setae and solenidion on tarsus I: *ft'* 10, *ft''* 8, *s* 7, *a''* 10, *u* 5, *p* 3, *e* 4, ω 5. Length of setae on femur II: *d* 19, *bv''* 8. Length of seta *l''* on genu II 8. Length of setae on tibia II: *d* 20–29, *l'* 14, *v'* 9–15. Length of setae and solenidion on tarsus II: *ft* 9–12, *u* 6–8, *p* 2, ω 2–3. Length of setae on femur III: *d* 14, *ev'* 6. Length of setae and solenidion on tibia III: *d* 15, ϕ 2. Length of setae on tarsus III: *ft''* 5, *u* 6, *p* 3. Length of seta *ev'* on femur IV 9. Length of setae on tibia IV: *d* 15, *v'* 6. Length of setae on tarsus IV: *u* 4, *ft''* 10, *p* 2.

Table 3 . Leg lengths of *Paralycus primus* sp. nov., holotype.

Leg	Trochanter	Femur	Genu	Tibia	Tarsus	All	Leg to body length ratio
I	10	28	14	16	25	93	≈0.5
II	7	20	10	11	20	68	≈0.36
III	11	12	10	11	22	66	≈0.35
IV	9	17	10	9	25	70	≈0.37

Note: Measurements are given in micrometers (μm) and are to be treated as minimal estimates.

Table 4 . Leg setation of *Paralycus primus* sp. nov., paratype.

Leg	Trochanter	Femur	Genu	Tibia	Tarsus
I	-	bv'' , d	(l) , v , d	l' , v' , φ	(ft) , a'' , s , (u) , (p) , ω , ε
II	-	bv'' , d	(l)	l' , v' , d	(ft) , (u) , (p) , ω
III	v'	ev' , d	-	v' , d	ft'' , (u) , (p)
IV	-	ev' , d	-	v' , d	ft'' , (u) , (p)

Note: Roman letters refer to normal setae, Greek letters refer to solenidia (except ε = famulus); d φ – coupled seta and solenidion. Single prime (') and double prime (") indicate setae on the anterior and posterior side of a segment, respectively. Parentheses indicate paired setae (' and ").

Etymology

The species epithet, *primus* (Latin adj., first), refers to *P. primus* as the oldest known species of *Paralycus*.

Remarks

In a single piece of amber, which contained a number of arthropod syninclusions, we found two complete specimens of *Paralycus*, and also a part of a possibly third specimen that was lost during preparation. The two complete specimens look very similar: setae in rows *f*, *h* and *p* long, extending beyond the bases of respective setae in the next row; presence of seta *4a*; elongated tarsus I. Considering these similarities and the finding of both specimens in a single piece of amber, we assume they are conspecific and combine their observable character states for our description. The differences in the lengths of some setae (f_1 , h_2 , p_1) may be attributed to their positioning at an angle to the image plane, making accurate measurement challenging. By the presence of four pairs of genital setae, *Paralycus primus* sp. nov. is similar to *P. parasiti* Zhang and Li, 2001, *P. pricei*, *P. aokii*, *P. shibai* Oshima and Shimano, 2024 and *P. subiasi* Oshima and Shimano, 2024. *Paralycus primus* sp. nov. differs from these species by notogastral setae d_1 and e_1 that reach the bases of the respective seta in the next posterior row (not reaching in the four other species) and rostral setae not reaching half the length of the chelicera (reaching half the length of the chelicera in the four other species, except *P. subiasi*). Additionally, *P. primus* sp. nov. differs from *P. pricei* by the presence of four setae on genu I (three setae in *P. pricei*), from *P. shibai* and *P. subiasi* by the presence of setae *4a* (absent in *P. shibai* and *P. subiasi*) and from *P. subiasi* by the presence of setae v' on trochanter III (absent in *P. subiasi*).

Discussion

The high quality of preservation has enabled us to describe the two fossil *Paralycus* species in sufficient detail for comparison with modern members of the genus. Despite their absolute and relative age differences—Middle Cretaceous (approximately 99 Mya) and Late Eocene (approximately 34 Mya)—the fossils exhibit all the characteristics of living *Paralycus* (see generic diagnosis of *Paralycus* in Kolesnikov *et al.* 2023), while also displaying enough differences to warrant their recognition as undescribed species. We conclude that *Paralycus* likely originated sometime before the Middle Cretaceous, since they share many similarities with contemporary species of the genus.

Possible phoresy

Both specimens of the Cretaceous *P. primus* sp. nov. were found as syninclusions with an unidentified wasp (Chrysidoidea). One mite was preserved in close proximity to the wasp's foreleg, potentially indicating phoresy (Fig. 14). Phoretic behaviour has also been observed

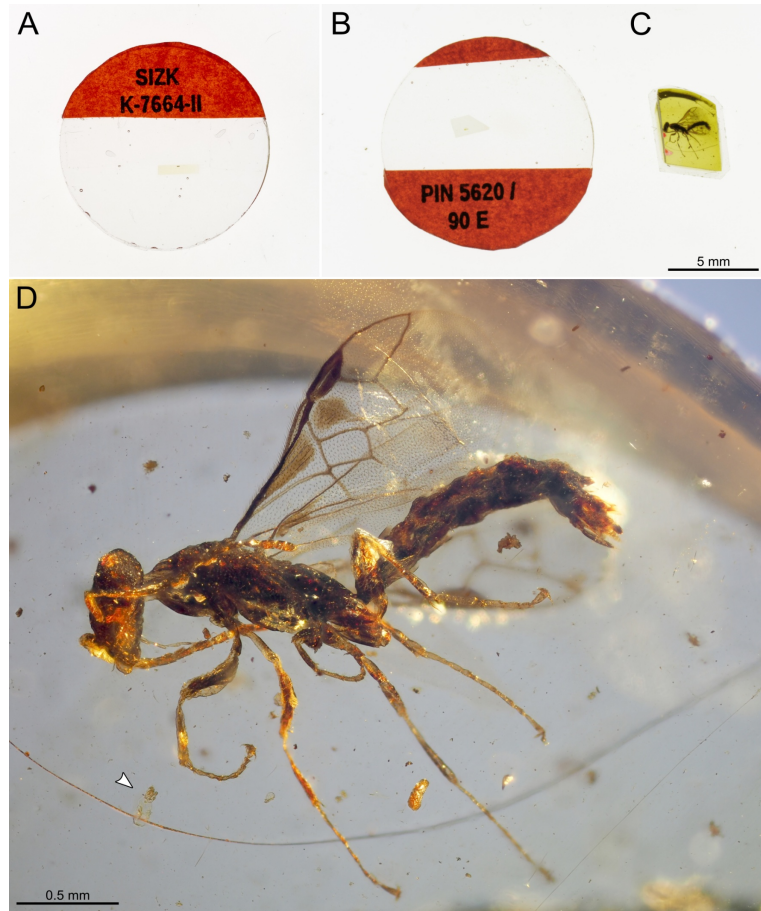


Figure 14 . Photographs of type specimens. A – SIZK K-7664-II, *Paralycus ekaterinae* sp. nov., holotype, piece of amber embedded in epoxy resin between two round glass coverslips; B – PIN 5620-90 E, *Paralycus primus* sp. nov., holotype, similar preparation as in A; C – piece of amber covered by epoxy resin containing PIN 5620-90 A (Hymenoptera Chrysoidea) and PIN 5620-90 D, *Paralycus primus* sp. nov., paratype; D – same as in C, enlarged, arrow points to the mite.

in some extant species of *Paralycus*, which have been reported as phoretic on vertebrates and insects. For instance, *P. raulti* and *P. pricei* have been found on the bees *Amegilla fallax* and *Apis mellifera* (Lavoipierre 1946), while *P. parasiti* has been recorded on the ladybird beetle *Coccinella septempunctata* (Zhang and Li 2001). Active phoresy among oribatid mites is relatively uncommon, primarily occurring in species associated with decaying wood and subcortical habitats (Norton 1980; Knee 2017, Klimov *et al.* 2021). In contrast, most soil-dwelling oribatid mites are more frequently found on avian feathers and mammalian hairs, where they likely engage in passive dispersal (Krivolutsky and Lebedeva 2002). Members of *Paralycus* do not exhibit distinct morphological adaptations for phoresy, such as specialized host attachment structures, like hook-like claws on the legs. The few documented instances of *Paralycus* phoresy lack details on the attachment mechanisms. It is plausible that these mites rely on simpler strategies, such as grasping host hairs or setae with their robust chelicerae or adhering to smooth surfaces of the host using their empodial pads. Given the broad range of substrates inhabited by Pediculochelidae and the variety of potential phoretic hosts, it is likely that their dispersal is opportunistic rather than host-specific. While the co-occurrence of *P. primus* sp. nov. with the wasp suggests phoresy as a potential pathway for the mites to become entrapped in amber, this relationship could also be incidental. If these mites lived on the bark of a resin-producing tree, as may be the case for *P. nortoni*, *P. aokii*, and *P. shibai* (Xu *et al.* 2020;

Oshima *et al.* 2024), the chances of being trapped in resin would have been high regardless of their association with other organisms.

Do amber imprints reflect the original shape and size of fossil animals?

The fossils described here raise the question of the size discrepancy between the imprint in amber and the smaller, apparently desiccated fossil inside it. This phenomenon has been documented in other amber fossils (Sidorchuk and Norton 2011; Moreau *et al.* 2017; Khaustov *et al.* 2021; Khaustov *et al.* 2024), where well-preserved cuticular parts sometimes display all the characters, including setal alveoli, in duplicate when viewed under transmitted light.

It is tempting to interpret the imprint as the true representation of the original mite's shape and size, attributing the discrepancy to the shrinkage of the dried cuticle (Schopf 1975; Gee *et al.* 2021), as discussed in relation to fossil oribatid mites (Sidorchuk and Norton 2011). This interpretation is occasionally supported by evidence of both shrinkage and breakage of the fossil cuticle, while the imprint retains minute details such as cuticular ornamentation. Sidorchuk and Norton (2011) concluded that the imprint generally preserves most setae, cerotegument, and accurate information on dimensions and proportions, except where distortion due to the death struggle is apparent. Given that the size of the imprint is often larger, it suggests that the remains of the animal have shrunk. Thus, the imprint is typically preferred for measurements rather than the cuticular remnants.

However, the imprint of *P. ekaterinae* **sp. nov.** presents a challenge to this generalization, as it displays disproportionately swollen legs I, including the setae, and possibly some gnathosomal structures (Fig. 1; see also Vorontsov and Voronezhskaya, 2022, and their Fig. 1). Inside the imprint, the cuticular remnants are visible, retaining more or less the normal proportions of leg I characteristic of *Paralycus*, and similar to other legs of the mite (albeit slightly shrunken). Two possible explanations arise: first, *P. ekaterinae* **sp. nov.** may have had disproportionately thicker legs I, which is atypical for the genus; second, the amber imprint may have expanded relative to the original shape of the mite. We consider the latter more likely. Notably, not only the leg segments appear thickened in the imprint, but also the setae originating from them. Since solid cuticular setae are unlikely to shrink and generally maintain a standard shape and thickness, at least within a single animal, the swollen contour of the imprint probably does not correspond to the original shape of the mite. Therefore, it must be acknowledged that neither the imprint nor the cuticular remnants can always be relied upon to reflect the original size of an organism accurately.

This conclusion adds uncertainty to the issue of precise measurements of amber fossils. However, we still endorse the recommendation of Sidorchuk and Norton (2011) that to capture all preserved details of an amber fossil, both the imprint and the cuticle remnants should be examined. Fortunately, various observational techniques are now available, including those used in this study, such as water immersion of amber specimens and confocal laser scanning microscopy (CLSM) of the fossil cuticle.

While we can only speculate on the reasons for the expansion of the amber imprint without a specific study, two possible explanations come to mind: (1) parts of the imprint may expand while the resin is not fully solidified, due to increased internal gas pressure from bacterial decomposition of the animal's tissues (McCoy *et al.* 2018); or (2) uneven evaporation of volatile components from the resin could lead to a decrease in volume, slightly expanding the dimensions of the internal hollow imprints.

Observation and imaging of minute fossils in amber

Both specimens of *P. primus* **sp. nov.** described here do not possess an imprint (air cavity), suggesting that their cuticles became fully impregnated with fossil resin. Consequently, they appear almost transparent, making these fossils challenging to detect when searching for inclusions under a dissecting microscope with reflected light. However, this transparency, which is a disadvantage for standard observation, becomes a significant advantage when

imaging the autofluorescence of cuticular structures using confocal laser scanning microscopy (CLSM). Fully impregnated amber fossils lack borders of optical density that would scatter light, enabling CLSM to produce high-resolution contrast images. Moreover, super-resolution adaptations of confocal microscopy, such as Airyscan (Huff 2015), offer enhanced resolution beyond the diffraction limit of light.

In this study, we applied CLSM, including Airyscan mode, to all our specimens and obtained high-resolution images that complemented observations made with transmitted light. For both specimens of *P. primus* **sp. nov.**, CLSM images were often more informative, especially for the paratype (PIN 5620-90 D), which was suboptimal for examination in transmitted light as it had not been separated from a larger piece of amber (Figure 7).

For the holotype of *P. ekaterinae* **sp. nov.**, Differential Interference Contrast (DIC) imaging failed to resolve the number of genital setae, despite several attempts on different microscopes. This issue arose because it was difficult to visually distinguish the image of the imprint from the remnants of the fossil tissue within it, which had higher optical contrast and obscured the view. Imaging the same specimen with Airyscan CLSM completely eliminated this uncertainty (Figure 2).

We strongly encourage researchers working with small fossils, particularly microarthropods, to use modern preparation techniques and imaging equipment like those described in Vorontsov *et al.* (2023). In many cases, it is the limitations of our instruments, rather than the quality of preservation, that constrain the level of morphological detail that can be resolved from amber fossils.

Acknowledgments


We thank Christoph Öhm-Kühnle (Tübingen, Germany), Alexander Rasnitsyn (Paleontological Institute RAS, Russia), and Evgeny Perkovsky (Schmalhausen Institute of Zoology, Ukraine) for providing the amber specimens used in this study. DDV is especially grateful to Christoph Öhm-Kühnle and Alexander Rasnitsyn, who gave permission to sacrifice the leg of an undescribed wasp during the separation of the mite, a risky operation that, fortunately, we managed to avoid. We are also very grateful to Evert Lindquist (Agriculture and Agri-Food Canada) for his initial identification of the mites shown to him by DDV, as well as for the fruitful discussions that followed. The CLSM images were taken using the equipment of the Core Centrum of the Institute of Developmental Biology, Russian Academy of Sciences. We extend our sincere thanks to Elena Voronezhskaya, head of the facility, for her invaluable assistance in optimizing the microscope's capabilities.

Funding

The work of DDV was conducted under the IDB RAS Government basic research program № 0088-2024-0011; VBK was funded by Ministry of Science and Higher Education of the Russian Federation within the framework of the Federal Scientific and Technical Program for the Development of Genetic Technologies for 2019–2027 (agreement № 075-15-2021-1345, unique identifier RF—193021X0012).

ORCID

Vasily B. Kolesnikov  <https://orcid.org/0000-0001-6177-7858>

Dmitry D. Vorontsov  <https://orcid.org/0000-0002-1701-1748>

Roy A. Norton  <https://orcid.org/0000-0001-9051-1450>

Pavel B. Klimov  <https://orcid.org/0000-0002-9966-969X>

References

- Baker E.W., Wharton G.W. 1952. An Introduction to Acarology. The Macmillan Co., N. Y. pp. 465.
- Berlese A. 1905. Acari nuovi. Materiali pel "Manipulus V". Redia, 2: 231-238.
- Coleman, C.O. 2006. Substituting time-consuming pencil drawings in arthropod taxonomy using stacks of digital photographs. Zootaxa, 1360: 61-68. <https://doi.org/10.11646/zootaxa.1360.1.4>
- Dunlop, J. A., Penney, D., Jekel, D. 2019. A summary list of fossil spiders and their relatives. World Spider Catalog, version 20.0. Updated at <http://wsc.nmbe.ch>, accessed 15 January 2019. doi:10.24436/2
- Fan Q.-H., Li L.-S., Xuan J.-Y. 1996. Two new species of the genus *Paralycus* from Sichuan, China (Acari: Pediculochelidae). Acta Zootaxonomica Sinica, 21 (2): 174-178. [in Chinese with English abstract]
- Gee, C. T., McCoy, V. E., Sander, P. M. 2021. Fossilization: Understanding the Material Nature of Ancient Plants and Animals. Johns Hopkins University Press. <https://books.google.ru/books?id=Ps4fEAAQBAJ>
- Huff, J. 2015. The Airyscan detector from ZEISS: confocal imaging with improved signal-to-noise ratio and super-resolution. Nature Methods, 12: 1-2. <https://doi.org/10.1038/nmeth.f.388>
- Khaustov, A. A., Lindquist, E. E., Perkovsky, E. E., Vasilenko, D. V., Vorontsov, D. D. 2024. Review of fossil heterostigmatic mites (Acari: Heterostigmata) from late Eocene Rovno Amber. II. Family Resinacaridae, with redescription of *Resinacarus resinatus* (Vitzthum), four new species and a new genus. Systematic and Applied Acarology, 29(9), 1244-1282. <https://doi.org/10.11158/saa.29.9.5>
- Khaustov, A. A., Vorontsov, D. D., Lindquist, E. E. 2024. The oldest evidence of symbiosis between mites and fungi with description of a new genus and species of Trochometriliidae (Acari: Heterostigmata) from Cretaceous amber. Systematic and Applied Acarology, 29(4): 475-500. <https://doi.org/10.11158/saa.29.4.3>
- Khaustov, A. A., Vorontsov, D. D., Perkovsky, E. E., Klimov, P. B. 2021a. First fossil record of mite family Barbutiidae (Acari: Raphignathoidea) from late Eocene Rovno Amber, with a replacement name *Hoplocheylus neosimilis* nomen novum (Tarsocheylidae). Systematic and Applied Acarology, 26(5): 973-980. <https://doi.org/10.11158/saa.26.5.12>
- Khaustov, A., Vorontsov, D., Perkovsky, E., Lindquist, E. 2021b. Review of fossil heterostigmatic mites (Acari: Heterostigmata) from late Eocene Rovno Amber. I. Families Tarsocheylidae, Dolichocybidae and Acarophenacidae. Systematic and Applied Acarology, 26(1): 33-61. <https://doi.org/10.11158/saa.26.1.3>
- Klimov, P. B., Khaustov, A. A., Vorontsov, D. D., Perkovsky, E. E., Pepato, A. R., Sidorchuk, E. A. 2020. Two new species of fossil Paratydeidae (Acari: Trombidiformes) from the late Eocene amber highlight ultraslow morphological evolution in a soil-inhabiting arthropod lineage. Journal of Systematic Palaeontology, 18(7): 607-629. <https://doi.org/10.1080/14772019.2019.1655496>
- Klimov P. B., Vorontsov D. D., Azar D., Sidorchuk E.A., Braig H.R., Khaustov A.A., Tolstikov A.V. 2021. A transitional fossil mite (Astigmata: Levantoglyphidae fam. n.) from the early Cretaceous suggests gradual evolution of phoresy-related metamorphosis. Scientific Reports 11 (1). <https://doi.org/10.1038/s41598-021-94367-2>
- Knee, W. 2017. A new *Paraleius* species (Acari, Oribatida, Scheloribatidae) associated with bark beetles (Curculionidae, Scolytinae) in Canada. ZooKeys, 667: 51-65. <https://doi.org/10.3897/zookeys.667.12104>
- Kolesnikov, V. B., OConnor, B., Ermilov, S. G., Klimov, P. B. 2023a. A review of the asexual mite genus *Paralycus* Womersley, 1944 (Acari: Oribatida: Pediculochelidae), with description of three new species and a key to species of the World. Diversity, 15(2): 160. <https://doi.org/10.3390/d15020160>
- Kolesnikov, V. B., Vorontsov, D. D., Perkovsky, E. E., Vasilenko, D. V., Klimov, P. B. 2023b. Confocal autofluorescence microscopy revealed the fine morphology of the amber preserved mite *Congovidia glesoconomorphi* sp. nov. (Acari: Hemisarcopidae) phoretic on a mycterid beetle. Palaeontology 006 (6): 665-678. <https://doi.org/10.11646/palaeontology.6.6.8>
- Kolesnikov, V. B., Vorontsov, D. D., Sidorchuk, E. A. 2024. Seven new species from Eocene Baltic amber reveal surprising diversity and suggest possible speciation scenarios in the relictual family Collohmanniidae (Acari: Oribatida). Zootaxa, 5553(1), 1-78. <https://doi.org/10.11646/zootaxa.5553.1.1>
- Krantz G. W. 1970. A manual of Acarology. Oregon State University Book Stores, Inc., Corvallis. pp. 335.
- Krivolutsky, D. A., Lebedeva, N. V. 2002. The oribatid mites and other microarthropods in the bird feathers. Studies on soil fauna in Central Europe. Institute of Soil Biology, Academy of Sciences, Ceske Budejovice, 101-104.
- Lavoipierre, M. 1946. A new acarine parasite of bees. Nature, 158 (4004): 130. doi:10.1038/158130b0 <https://doi.org/10.1038/158130b0>
- Lindquist, E., Vorontsov, D. D. 2023. *Uropodella* (Acari: Mesostigmata: Sejidae), mites unchanged from Eocene past to Holocene present. Acarologia, 63(2): 346-355. <https://doi.org/10.24349/y1ey-edzd>
- McCoy, V. E., Soriano, C., Pegoraro, M., Luo, T., Boom, A., Foxman, B., Gabbott, S. E. 2018. Unlocking preservation bias in the amber insect fossil record through experimental decay. PLoS One, 13(4), e0195482. <https://doi.org/10.1371/journal.pone.0195482>
- Moreau, J. D., Néraudeau, D., Perrichot, V., Tafforeau, P. 2017. 100-million-year-old conifer tissues from the mid-Cretaceous amber of Charente (western France) revealed by synchrotron microtomography. Annals of Botany, 119(1): 117-128. <https://doi.org/10.1093/aob/mcw225>
- Norton R. A., OConnor B. M., Johnston D. E. 1983. Systematic relationships of the Pediculochelidae (Acari: Acariformes). Proceedings of the Entomological Society of Washington, 85 (3): 493-512.
- Norton, R. A. 1980. Observations on phoresy by oribatid mites (Acari: Oribatei). International Journal of Acarology, 6(2): 121-130. <https://doi.org/10.1080/01647958008683206>
- Oshima, M., Nakano, T., Shimano, S. 2024. Two new species of the genus *Paralycus* Womersley, 1944 (Oribatida, Pediculochelidae) from Japan. Edaphologia, 115: 83-95. <https://doi.org/10.11646/zootaxa.5556.1.16>

- Oshima, M., Shimano, S. 2024. A new species of the genus *Paralycus* Womersley, 1944 (Acari, Oribatida, Pediculochelidae) from Shikoku-island, Japan. *Zootaxa* 5556 (1): 218-225. <https://doi.org/10.11646/zootaxa.5556.1.16>
- Pepato, A. R., Klimov, P. B. 2015. Origin and higher-level diversification of acariform mites - evidence from nuclear ribosomal genes, extensive taxon sampling, and secondary structure alignment. *Evolutionary Biology*, 15:178. <https://doi.org/10.1186/s12862-015-0458-2>
- Perkovsky, E.E., Zosimovich, V.Y., Vlaskin, A.P. 2010. Rovno Amber. In: Penney, D. (Eds.), Biodiversity of fossils in amber from the major world deposits. Manchester, Siri Scientific Press, pp. 116-136.
- Price D. W. 1973. Genus *Pediculocheilus* (Acarina: Pediculochelidae), with notes on *P. raulti* and descriptions of two new species. *Annals of the Entomological Society of America*, 66 (2), 302-307. doi:10.1093/aesa/66.2.302 <https://doi.org/10.1093/aesa/66.2.302>
- Radchenko, A.G., Perkovsky, E.E., Vasilenko, D.V. 2021. *Formica* species (Hymenoptera, Formicidae, Formicinae) in late Eocene Rovno amber. *Journal of Hymenoptera Research*, 82: 237-251. <https://doi.org/10.3897/jhr.82.64599>
- Schindelin, J., Arganda-Carreras, I., Frise, E., Kaynig, V., Longair, M., Pietzsch, T., Preibisch, S., Rueden, C., Saalfeld, S., Schmid, B., Tinevez, J.-Y., White, D.J., Hartenstein, V., Eliceiri, K., Tomancak, P., Cardona, A. 2012. Fiji: an open-source platform for biological-image analysis. *Nature Methods* 9: 676-682. <https://doi.org/10.1038/nmeth.2019>
- Schopf, J. M. 1975. Modes of fossil preservation. *Review of Palaeobotany and Palynology*, 20(1-2): 27-53. [https://doi.org/10.1016/0034-6667\(75\)90005-6](https://doi.org/10.1016/0034-6667(75)90005-6)
- Sellnick, M. 1931. Milben im Bernstein. *Bernstein-Forschungen*, 2: 148-180.
- Shi, G.H., Grimaldi, D.A., Harlow, G.E., Wang, J., Wang, J., Yang, M., Lei, W., Li, Q., Li, X. 2012. Age constraint on Burmese amber based on U-Pb dating of zircons. *Cretaceous Research*, 37: 155-163. <https://doi.org/10.1016/j.cretres.2012.03.014>
- Sidorchuk, E. A. 2018. Mites as fossils: forever small? *International Journal of Acarology*, 44: 349-359. <https://doi.org/10.1080/01647954.2018.1497085>
- Sidorchuk, E.A., Norton R.A. 2011. The fossil mite family Archaeorchestidae (Acari, Oribatida) I: redescription of *Strieremaeus illibatus* and synonymy of *Strieremaeus* with *Archaeorchestes*. *Zootaxa* 2993: 34-58 <https://doi.org/10.11646/zootaxa.2993.1.3>
- Sidorchuk, E.A., Vorontsov, D.D. 2018. Preparation of small-sized 3D amber samples: state of the technique. *Palaeoentomology*, 1: 80-90. <https://doi.org/10.11646/palaeoentomology.1.1.10>
- Smith, R.D.A., Ross, A.J., 2018. Amberground pholadid bivalve borings and inclusions in Burmese amber: implications for proximity of resin-producing forests to brackish waters, and the age of the amber. *Earth and Environmental Science Transactions of the Royal Society of Edinburgh* 107 (2-3): 239-247. <https://doi.org/10.1017/S1755691017000287>
- Sokoloff, D.D., Ignatov, M.S., Remizowa, M.V., Nuraliev, M.S., Blagoderov, V., Garbout, A., Perkovsky, E.E. 2018. Staminate flower of *Prunus s. l.* (Rosaceae) from Eocene Rovno amber (Ukraine). *Journal of Plant Research*, 131 (6): 925-943. <https://doi.org/10.1007/s10265-018-1057-2>
- Vorontsov, D., Voronezhskaya, E. E. 2022. Pushing the limits of optical resolution in the study of the tiniest fossil arthropods. *Historical Biology*, 34(12), 2415-2423. <https://doi.org/10.1080/08912963.2021.2017920>
- Vorontsov, D.D., Kolesnikov, V.B., Voronezhskaya, E.E., Perkovsky, E.E., Berto, M.M., Mowery, J., Ochoa, R., Klimov, P.B. 2023. Beyond the Limits of Light: An Application of Super-Resolution Confocal Microscopy (sCLSM) to Investigate Eocene Amber Microfossils. *Life* 13(4): 865. <https://doi.org/10.3390/life13040865>
- Xu Y., Zhu Y.-Z., Wu J.-Q., Zhang F.-P. 2020 A new species of the genus *Paralycus* from Fujian, China. *Acarologia*, 60(2): 481-487. <https://doi.org/10.24349/acarologia/20204377>
- Yu, T.T., Kelly, R., Mu, L., Ross, A., Kennedy, J., Broly, P., Xia, F.Y., Zhang, H.C., Wang, B., Dilcher, D. 2019. An ammonite trapped in Burmese amber. *Proceeding of the National Academy of Sciences of United States of America* 116 (23): 11345-11350. <https://doi.org/10.1073/pnas.1821292116>
- Zhang A.-H., Li Y.-R. 2001. A new species of the genus *Paralycus* from Chongqing, China. *Journal of Southwest Agricultural University*, 23 (4): 317-318. [in Chinese with English abstract].
- Zhang, Q., Rasnitsyn, A. P., Wang, B., Zhang, H.C. 2018. Hymenoptera (wasps, bees and ants) in mid-Cretaceous Burmese amber: A review of the fauna. *Proceedings of the Geologists' Association* 129: 736-747. <https://doi.org/10.1016/j.pgeola.2018.06.004>